SHEP-07-29
DFTT 39/2009 November 17, 2010

Production of Light Higgs Pairs in 2-Higgs Doublet Models via the Higgs-strahlung Process at the LHC

M. Moretti
Dipartimento di Fisica, Università di Ferrara and
INFN - Sezione di Ferrara, Via Paradiso 12, 44100 Ferrara, Italy

S. Moretti
School of Physics & Astronomy, University of Southampton,
Highfield, Southampton SO17 1BJ, UK

and

Dipartimento di Fisica Teorica, Università degli Studi di Torino
Via Pietro Giuria 1, 10125 Torino, Italy

F. Piccinini
INFN - Sezione di Pavia,
Via Bassi 6, 27100 Pavia, Italy

R. Pittau
Departamento de Física Teórica y del Cosmos and Centro Andaluz de Física de Partículas Elementares (CAFPE), Universidad de Granada, E-18071 Granada, Spain

J. Rathsman
Department of Physics and Astronomy, Uppsala University,
PO Box 516, 751 20 Uppsala, Sweden

Abstract

At the Large Hadron Collider, we prove the feasibility to detect pair production of the lightest CP-even Higgs boson h of a Type II 2-Higgs Doublet Model through the process $q\bar{q}^{(\prime)} \to Vhh$ (Higgs-strahlung, $V = W^{\pm}, Z$), in presence of two $h \to b\bar{b}$ decays. We also show that, through such production and decay channels, one has direct access to the following Higgs self-couplings, thus enabling one to distinguish between a standard and the Supersymmetric version of the above model: λ_{Hhh} – which constrains the form of the Higgs potential – as well as $\lambda_{W^{\pm}H^{\mp}h}$ and λ_{ZAh} – which are required by gauge invariance. Unfortunately, such claims cannot be extended to the Minimal Supersymmetric Standard Model, where the extraction of the same signals is impossible.

1 Introduction

The ability to access Higgs self-couplings would enable one to constrain the form of the Higgs potential responsible for Electro-Weak Symmetry Breaking (EWSB) and, in particular, to assess whether such a potential corresponds to the one embodied in the Standard Model (SM) or indeed in extended versions of it. Lately, amongst the scenarios with an enlarged Higgs sector, much attention has been devoted to a (CP-conserving) Type II 2-Higgs Doublet Model (2HDM), possibly in presence of minimal Supersymmetry (SUSY) – the combination of the two yielding the so-called Minimal Supersymmetric Standard Model (MSSM) [1]. In a generic 2HDM and in the MSSM, of the initial eight degrees of freedom pertaining to the two complex Higgs doublets, only five survive as real particles upon EWSB, labelled as h, H, A (the first two are CP-even or 'scalars' (with $M_h < M_H$) whereas the third is CP-odd or 'pseudoscalar') and $H^\pm$, as three degrees of freedom are absorbed into the definition of the longitudinal polarisation for the gauge bosons Z and $W^\pm$, upon their mass generation after EWSB. This thus makes four additional Higgs particle states with respect to the SM, wherein only one complex Higgs doublet is allowed which, after EWSB, generates a lone CP-even (scalar) Higgs boson (henceforth also denoted by h).

The detection of a h state, independently of the underlying model (amongst those mentioned), is guaranteed at the Large Hadron Collider (LHC) [2, 3, 4], over the theoretically allowed mass intervals. However, notice that while the Higgs boson mass M_h is a free parameter in both the SM and a generic 2HDM, so that its upper limit (of about 700 GeV) is only dictated by unitarity requirements, in the MSSM the SUSY relations interlinking gauge and Higgs couplings imply an absolute upper limit on the mass of the lightest Higgs boson M_h of about 140 GeV (see the second paper in [2] and references therein). Furthermore, there is a lower limit from LEP, of about 115 GeV, applicable directly to M_h in the SM but also adoptable in both a generic 2HDM and the MSSM over large areas of their parameter spaces. Finally, the Tevatron has put an exclusion limit on M_h in the SM in the range 162-166 GeV [5].

The CP-conserving 2HDM, with soft Z_2 symmetry breaking, is identified uniquely at tree level by seven independent parameters (as will be made clear below): M_h, M_H, M_A, $M_{H^\pm}$, $\tan\beta$ (the ratio between the vacuum expectation values of the two Higgs doublets), α (the mixing angle between the two CP-even neutral Higgs states) and $\lambda_5 = (\Lambda_5 - \Lambda_6)/2$, one of the parameters of the Higgs potential as defined in [6] (see also [7]). In the case of the MSSM, at tree level, only two parameters are needed, $\tan\beta$ and any of the Higgs masses (henceforth M_A). (Recall that, in the SM, M_h is the only free parameter in the Higgs potential.)

An intriguing situation that could arise at the LHC is then the following. That only a light Higgs state, with mass below 140 GeV, is found and it is impossible to establish whether

it belongs to the SM, a generic 2HDM or indeed the MSSM. In fact, this happens in the so-called 'decoupling region' of the extended scenarios, i.e., when $M_H, M_A, M_{H^\pm} \gg M_h$ (and for suitable choices of the additional free inputs in the generic 2HDM), quite independently of $\tan\beta$, where - for the same mass - the h couplings to ordinary matter in the SM are the same as those in both the 2HDM and MSSM[1]. Even in these conditions, however, it has been proved that one could possibly establish the presence of an extended Higgs sector by determining the size of the trilinear Higgs self-coupling λ_{hhh} [8], by looking at the Vector Boson Fusion (VBF) process, $qq^{(\prime)} \to qq^{(\prime)}hh$, and possibly also distinguish between a generic 2HDM and the MSSM by isolating the λ_{Hhh} trilinear Higgs self-coupling in the same VBF channel [9]. This can be achieved by looking at decays of the two light Higgs states produced into bottom-quark pairs.

In general though, this distinction between a generic 2HDM and the MSSM is not always possible. Not even the discovery of also the A and $H^\pm$ states may say the conclusive word in this respect. In fact, despite there exist well established spectra among the four different masses in the MSSM (dictated indeed by SUSY for fixed, say, M_h and $\tan\beta$), it may well be possible that the additional 2HDM parameters arrange themselves to produce an identical mass pattern. However, such a degeneracy between the two models would not typically persist if one were able to also measure other Higgs-gauge couplings, chiefly $\lambda_{W^\pm H^\mp h}$ and/or λ_{ZAh}, which are both proportional to $\cos(\beta-\alpha)$ times gauge couplings. Even though the form of the Higgs-gauge coupling is specified by reasons of gauge invariance, the actual size can be different in the MSSM and in a generic 2HDM since in the latter both α and β are independent parameters. Hence, the measurement of at least one of these Higgs-gauge couplings would constitute a confirmation, or otherwise, of the MSSM relations if one knew M_h (and possibly the heavier masses, M_H, M_A plus $M_{H^\pm}$) and $\tan\beta$ but not α.

These Higgs-gauge couplings are accessible via the double Higgs-strahlung process, that we intend to study here[2]. Our approach is very conservative, as we make the assumption that only one parameter is known, M_h, measured for some value below 140 GeV, as may well happen at the LHC after only a h resonance is detected. We further imply that all SUSY states are much heavier than ordinary particles (with the possible exception of the lightest SUSY particle, which may well escape detection) and not yet detected by the time the h resonance is isolated and our advocated studies are pursued. In particular, in this paper, we show that, by resorting to double Higgs-strahlung, it is possible to extract both $\lambda_{W^\pm H^\mp h}$

[1]In the MSSM, one also has to presume that the sparticle states are very heavy, so that the existence of a SUSY scenario is not obviously manifest through their detection.

[2]In principle, they can also be accessed in VBF: see the last four graphs of Fig. 1 in [9]. In practise, we had verified in that paper that the contribution due to those diagrams was not accessible, the main reason being that they are not resonant in VBF, unlike the case of Higgs-strahlung.

and λ_{ZAh} in a generic 2HDM whilst in the MSSM neither of them is accessible[3].

Therefore, in conjunction with the measurement of λ_{Hhh}, accessible in VBF [9] and also in the process considered here (as we shall show), one will in principle be able to disentangle between the 2HDM and the MSSM, even if only a light Higgs resonance is found after earlier LHC data and no SUSY states are visible throughout. However, all this phenomenology requires that enough luminosity can be accumulated at the LHC, such that the Super-LHC (SLHC) option [11] becomes needed to perform such kind of studies.

We will illustrate how we have come to this conclusion, i.e., after investigating the production of lightest Higgs boson pairs in the Higgs-strahlung process, namely [12, 13]:

$$q\bar{q}^{(\prime)} \to Vhh, \tag{1}$$

with $V = W^{\pm}$ or Z and $q^{(\prime)}$ referring to any possible (anti)quark flavour. The relevant Feynman diagrams corresponding to this channel in both the 2HDM and MSSM considered here can be found in Fig. 1. (Herein, notice the three graphs at the bottom, where the λ_{hhh} or λ_{Hhh} and $\lambda_{W^{\pm}H^{\mp}h}$ or λ_{ZAh} couplings are located.) In our selection analysis, we will resort to the extraction of two $h \to b\bar{b}$ resonances, in presence of both hadronic and leptonic V decays, i.e., we will study the following signatures:

1. 'four b-quark jets and two light-quark jets', emerging from (1) if $W^{\pm}, Z \to$ jet-jet;

2. 'four b-quark jets and a lepton pair', emerging from (1) if $Z \to \ell^+\ell^-$;

3. 'four b-quark jets, one lepton and missing energy', emerging from (1) if $W^{\pm} \to \ell^{\pm}\nu_{\ell}$.

We will limit ourselves to the case $\ell = e, \mu$ and we will discuss the procedure to tag the b-jets.

Our paper is organised as follows. In the next section, we outline the computational procedure. Sect. 3 presents our numerical results and discusses these. Sect. 4 contains our conclusions.

2 Calculation

We have assumed $\sqrt{s} = 14$ TeV for the LHC energy throughout. Our numerical results are obtained by setting the renormalisation and factorisation scales to $2M_h$ for the signal while for the QCD background we have used the average jet transverse momentum ($p_T^2 = \sum_1^n p_{Tj}^2/n$). Both Higgs processes and noise were estimated by using the Parton Distribution Function (PDF) set MRST99(COR01) [14]. All signal and background calculations were based on

[3]Similar conclusions also hold at linear colliders, as shown in Ref. [10].

exact tree-level Matrix Elements (MEs) using either the ALPGEN program [15] or the HELAS subroutines [16]. Furthermore, VEGAS [17] or Metropolis [18] were used for the multi-dimensional integrations over the phase space. As for numerical input values of SM parameters, we adopted the ALPGEN defaults.

Concerning the MSSM setup, the two independent tree-level parameters that we adopt are M_A and $\tan\beta$. Through higher orders, we have considered the so called 'Maximal Mixing' scenario ($X_t = A_t - \mu/\tan\beta = \sqrt{6}M_{\rm SUSY}$) [19], wherein we have chosen for the relevant SUSY input parameters: $\mu = 200$ GeV, $A_b = 0$, with $M_{\rm SUSY} = 5$ TeV, the latter – as already intimated – implying a sufficiently heavy scale for all sparticle masses, so that these are not accessible at the LHC and no significant interplay between the SUSY and Higgs sectors of the model can take place[4]. Masses and couplings within the MSSM have been obtained by using the HDECAY program [20]. The $\tan\beta$ and M_A values adopted as representative of the MSSM parameter space were: $\tan\beta = 3$ and 40 for $M_A = 160$, 200 and 240 GeV (yielding $M_{h,H} = 108(178)$ GeV, $M_{h,H} = 112(212)$ GeV and $M_{h,H} = 114(249)$ GeV for the low $\tan\beta$ value plus $M_{h,H} = 129(160)$ GeV, $M_{h,H} = 129(200)$ GeV and $M_{h,H} = 129(240)$ GeV for the high one, respectively).

Before giving the details of the 2HDM setup we are using, let us recall the most general CP-conserving 2HDM scalar potential which is (Z_2) symmetric under $\Phi_{1(2)} \to -(+)\Phi_{1(2)}$ up to softly breaking dimension-2 terms (thereby allowing for loop-induced flavour changing neutral currents) [1],

$$\begin{aligned} V &= m_{11}^2\Phi_1^\dagger\Phi_1 + m_{22}^2\Phi_2^\dagger\Phi_2 - \left\{m_{12}^2\Phi_1^\dagger\Phi_2 + h.c.\right\} + \frac{1}{2}\lambda_1\left(\Phi_1^\dagger\Phi_1\right)^2 + \frac{1}{2}\lambda_2\left(\Phi_2^\dagger\Phi_2\right)^2 + \\ &\quad + \lambda_3\left(\Phi_1^\dagger\Phi_1\right)\left(\Phi_2^\dagger\Phi_2\right) + \lambda_4\left(\Phi_1^\dagger\Phi_2\right)\left(\Phi_2^\dagger\Phi_1\right) + \left\{\frac{1}{2}\lambda_5\left(\Phi_1^\dagger\Phi_2\right)^2 + h.c.\right\}. \end{aligned} \tag{2}$$

In the following, the parameters m_{11}, m_{22}, m_{12}, λ_1, λ_2, λ_3 and λ_4 are replaced by v, M_h, M_H, M_A, $M_{H^\pm}$, β and α (with v fixed). Hence, as intimated already, the CP-conserving 2HDM potential is parameterised by seven free parameters. Notice that from the scalar potential all the different Higgs couplings needed for our study can easily be obtained. (See [6, 7] for a complete compilation of couplings in a general CP-conserving 2HDM.) In addition, since we are considering a so called Type II 2HDM the Yukawa couplings are also fixed by $\tan\beta$ in the same way as in the MSSM.

In our 2HDM, we will fix M_h and M_H to values similar to the ones found in the MSSM scenario we are considering, by adopting three different setups:

[4]The only possible exception in this mass hierarchy would be the Lightest Supersymmetric Particle (LSP), as intimated already, whose mass may well be smaller than the lightest Higgs mass values that we will be considering. However, we have verified that invisible h decays (including the one into two LSPs) have negligible decay rates.

1. $M_h = 115$ GeV, $M_H = 250$ GeV, $M_A = 220$ GeV, $M_{H^\pm} = 300$ GeV,

2. $M_h = 115$ GeV, $M_H = 300$ GeV, $M_A = 305$ GeV, $M_{H^\pm} = 310$ GeV,

3. $M_h = 115$ GeV, $M_H = 400$ GeV, $M_A = 405$ GeV, $M_{H^\pm} = 410$ GeV,

where in the first scenario the masses have been chosen such that $M_H > 2M_h$, $M_A > M_h + M_Z$ and $M_{H^\pm}$ is above the limit given by measurements of $b \to s\gamma$ (for recent limits see [21, 22] and references therein).

We always scan over the remaining parameters in the ranges

$$-\pi/2 < \alpha < \pi/2,$$
$$-4\pi < \lambda_5 < 4\pi,$$
$$0 < \tan\beta < 50.$$

In order to accept a point from the scan we also check that the following conditions are fulfilled: the potential is bounded from below, the λ_i's comply with the unitarity constraints of [23] and yield a contribution to $|\Delta\rho| < 10^{-3}$. In short, the unitarity constraints amount to putting limits on the eigenvalues of the S matrices for the scattering of various combinations of Higgs and EW gauge bosons. We have followed the normal procedure [1] of requiring the $J = 0$ partial waves (a_0) of the different scattering processes to fulfill $|\mathrm{Re}(a_0)| < 1/2$, which corresponds to applying the condition that the eigenvalues[5] $\Lambda^{Z_2}_{Y\sigma^\pm}$ of the scattering matrices (or more precisely $16\pi S$) fulfill $|\Lambda^{Z_2}_{Y\sigma^\pm}| < 8\pi$ [24]. In other words we allow parameter space points all the way up to the tree-level unitarity constraint $|\mathrm{Re}(a_0)| < 1/2$. The spectrum of masses, couplings and decay rates in our 2HDM is similar to the one exploited in Ref. [9][6], obtained by using a modification of HDECAY [20] (consistent with a similar manipulation of the program used in Ref. [41]). For each accepted point in the scan the partial decay rates for the different Higgs bosons are then calculated using such HDECAY modification and also taking possible additional (i.e., 2HDM specific) partial widths of the H, A, and $H^\pm$ bosons into account. We have also cross-checked the results by using the 2HDMC program [42] to perform the same calculations. The results of the above discussed constraints on the parameter space are shown in Fig. 2, where the projections of the allowed parameters on three different planes, λ_5–$\tan\beta$, $\sin(\beta-\alpha)$–$\tan\beta$ and $\sin(\beta-\alpha)$–λ_5, with a sample of 1000 randomly chosen points are plotted. It is worth noting that the allowed region in the plane λ_5–$\tan\beta$ complies with the constraints found in Refs. [38, 43], where the neutral Higgs-pair production and Higgs-strahlung at linear colliders within the general 2HDM have been investigated at the one-loop level.

[5]Here, Z_2 refers to the Z_2 symmetry, Y is the hypercharge, and $\vec{\sigma}$ is the total weak isospin.

[6]For a variety of studies of Higgs pair production at the LHC, primarily through gluon-gluon fusion, see Refs. [25]–[37]. Recent studies at linear and $\gamma\gamma$ colliders can be found in Refs. [38], [39] and [40].

While the parameter dependence of the MSSM Higgs sector renders the computation of the tree-level MSSM cross-sections rather straightforward (as the latter depends on two parameters only, M_A and $\tan\beta$), the task becomes much more time-consuming in the context of the 2HDM. In order to calculate the cross-sections in this scenario, the latter are written as a combination of couplings and kinematic factors in the following way ($n = 5$):

$$\sigma_{\rm tot} = \int \left| \sum_{i=1}^{n} g_i M_i \right|^2 d\text{LIPS} = \sum_{i=1}^{n} \sum_{j=i}^{n} g_i g_j \sigma_{ij}, \tag{3}$$

where all the explicit dependence on α, β, λ_{Hhh} and λ_{hhh} is contained in the couplings g_i: $g_1 = \sin^2(\beta-\alpha)$, $g_2 = \cos^2(\beta-\alpha)$, $g_3 = \cos(\beta-\alpha)\lambda_{Hhh}$, $g_4 = \sin(\beta-\alpha)\lambda_{hhh}$, and $g_5 = 1$, whereas the dependence on masses and other couplings is in the factors

$$\sigma_{ij} = \frac{1}{1+\delta_{ij}} \int \left(M_i^\dagger M_j + M_j^\dagger M_i \right) d\text{LIPS}. \tag{4}$$

Note that the sum over subamplitudes M_i also contains all interference terms and that colour factors etc. are included properly. The σ_{ij} are then calculated numerically for fixed masses. We can then get the cross-section in an arbitrary parameter space point by multiplying the kinematic factors with the appropriate couplings. However, there is a slight complication since the kinematic factor for the $H \to hh$ contribution depends on the width Γ_H if there is a s-channel resonance and the width in turn depends on the couplings. In this case the kinematic factor scales as $1/\Gamma_H$ which is accounted for by assuming a fixed value for the width when the kinematic factor is calculated and then rescaling the result with the true width when calculating the contribution to the cross-section. The same type of procedure is also applied for the $A \to Zh$ and $H^\pm \to W^\pm h$ resonant contributions.

Notice that such a procedure, after the summation in eq. (3), amounts to the exact (i.e., complete and gauge invariant[7]) calculation of the cross section for process (1).

3 Results

3.1 Inclusive Signal Results

In this section, after a preliminary analysis of the Higgs mass and coupling spectra in the MSSM and a general Type II 2HDM, we will start our numerical analysis by investigating the model parameter dependence of the Higgs pair production process in (1) at fully inclusive level, assuming on-shell production of gauge and Higgs bosons, followed by the decay of the former in all possible final states (of quarks, leptons and neutrinos, as appropriate) and of

[7]Apart from subleading effects of $\mathcal{O}(\Gamma/M)$, where M and Γ are the mass and width, respectively, of a resonant particle.

the latter into two $b\bar{b}$ pairs, with the integration over the phase space being performed with no kinematical restrictions. This will be followed by an analysis of the production and decay processes pertaining to the Higgs signals at fully differential level, in presence of detector acceptance cuts and kinematical selection constraints. Finally, we will compare the yield of the signals to that of the corresponding backgrounds and perform a dedicate signal-to-background study including an optimisation of the cuts in order to enhance the overall signal significance. We will treat the MSSM and 2HDM in two separate subsections.

3.1.1 MSSM

As representative of the low and high $\tan\beta$ regime, we will use in the remainder the values of 3 and 40. We have instead treated M_A as a continuous parameter, varying between 100 and 700 GeV or so[8]. Fig. 3 presents the fully inclusive MSSM cross-section for the process of interest, as defined in (1), followed by two $h \to b\bar{b}$ decays and of those of the $W^\pm$ and Z bosons into anything. In the same figure, we also show the rates corresponding to the case in which we have removed from the list of diagrams the last two in Fig. 1[9], in order to individuate the origin of possible dynamic structures. In fact, the difference between the red and black lines illustrate the effects of the diagrams involving the $\lambda_{W^\pm H^\mp h}$ and λ_{ZAh} couplings, which can amount to a resonant contribution (at low $\tan\beta$) or a constructive interference (at large $\tan\beta$).

The displayed rates however correspond to the ideal situation in which all final state objects (quarks and gauge bosons) are detected with unit efficiency and the detector coverage extends to their entire phase space, so that they only serve as a guidance in rating the phenomenological relevance of the processes discussed.

A more realistic analysis is in order, which we have performed as follows. In all channels, the four b-jets emerging from the decay of the hh pair are accepted according to the following criteria:

$$p_T^b > 30 \text{ GeV}, \qquad |\eta^b| < 2.5, \qquad \Delta R_{bb} > 0.7. \tag{5}$$

Their tagging efficiency is taken as $\epsilon_b = 50\%$ for each b satisfying these requirements, $\epsilon_b = 0$ otherwise[10]. We assume no b-jet charge determination. In addition, to enforce the reconstruction of the two Higgs bosons, we require all such b's in the event to be tagged and that at least one out of the three possible double pairings of b-jets satisfies the following mass

[8]Values of M_A below 90 GeV or so are actually excluded by LEP for the lower $\tan\beta$ value: see [44].

[9]Notice in fact that the two sets of diagrams peak in different phase space regions, so that, modulo the aforementioned $\mathcal{O}(\Gamma/M)$ effects, they can safely be separated.

[10]Here and in the remainder, the label b refers to jets that are b-tagged while j to any jet (even those originating from b-quarks) which is not. As probability for a gluon or light-quark jet to fake a b jet we take $R = 1/100$.

preselection:

$$(m_{b_1,b_2} - M_h)^2 + (m_{b_3,b_4} - M_h)^2 < 2\ \sigma_m^2, \tag{6}$$

where $\sigma_m = 0.12\ M_h$ whereas b_1b_2 and b_3b_4 refer, hereafter, to the two pairs of b-jets best reconstructing the Higgs masses with b_1 being the b-jet with highest p_T. (As intimated, we will be working under the assumption that a light Higgs state h is found already.)

As for tagging the gauge bosons produced via the Higgs-strahlung process (1), there are two possibilities, depending on whether the gauge boson decays are 'leptonic' or 'hadronic'. In the former case, the additional cuts are

$$p_T^{\ell,\rm miss} > 20\ \text{GeV}, \qquad |\eta^{\ell,\rm miss}| < 2.5, \qquad \Delta R_{b\ell,b\rm miss} > 0.4, \qquad |M_{\ell^+\ell^-} - M_Z| < 5\ \text{GeV} \tag{7}$$

(with $\ell = e, \mu$ and wherein the neutrino transverse momentum is equated to the missing one, $p_T^{\rm miss}$, while the longitudinal one is reconstructed by assuming $M_{\ell\nu_\ell} \equiv M_{W^\pm}$ and choosing the solution with smallest magnitude). In the latter case, we use

$$p_T^j > 20\ \text{GeV}, \qquad |\eta^j| < 2.5, \qquad \Delta R_{bj,jj} > 0.7, \qquad 70\ \text{GeV} < M_{jj} < 100\ \text{GeV}, \tag{8}$$

where M_{jj} is the invariant mass of the two non-b-jets in the event.

In our investigation of hadronic final states, we will assume that b-quark jets are distinguishable from light-quark and gluon ones and, as already mentioned, neglect considering b-jet charge determination. In the case of leptonic ones, we will limit ourselves to the case of electrons and muons (collectively denoted by the symbol ℓ). Finite calorimeter resolution has been emulated through a Gaussian smearing in transverse momentum, p_T, with $(\sigma(p_T)/p_T)^2 = (0.60/\sqrt{p_T})^2 + (0.04)^2$ for all jets and $(\sigma(p_T)/p_T)^2 = (0.12/\sqrt{p_T})^2 + (0.01)^2$ for leptons. The corresponding missing transverse momentum, $p_T^{\rm miss}$, was reconstructed from the vector sum of the visible momenta after resolution smearing. Also, in our parton level analysis, we have identified jets with the partons from which they originate and applied all cuts directly to the latter, since parton shower and hadronisation effects were not included in our study.

Tab. 1 shows the rates of the signal after the implementation of the acceptance and preselection cuts in eqs. (5)–(8) (hereafter, also referred to as 'primary cuts'). Notice that b-tagging efficiencies are not taken into account in this table. In fact, for the '4b-jet' tagging option that we are advocating, one should multiply the numbers in Tab. 1 by ϵ_b^4, that is, 1/16.

The conclusion here is rather straightforward: given the smallness of the inclusive signal rates, the scope of extracting $hh \to 4b$ signals in the MSSM from the double Higgs-strahlung process (1) is basically nil. Therefore, in our forthcoming signal-to-background analysis, we will not pursue the MSSM case.

M_A (GeV)	$\sigma(q\bar{q}^{(\prime)} \to Vhh)$ (fb)
160	0.028(0.034)
200	0.019(0.037)
240	0.022(0.053)
$\tan\beta = 3$	
160	0.013(0.031)
200	0.011(0.024)
240	0.0087(0.020)
$\tan\beta = 40$	

Table 1: Cross-sections for Higgs-strahlung after Higgs/gauge boson decays (relevant Branching Ratios (BRs) are all included) and the acceptance and preselection cuts defined in (5)–(8), for two choices of $\tan\beta$ and a selection of M_A values, assuming the MSSM in Maximal Mixing configuration. Here, the numbers outside(inside) brackets refer to the 'leptonic'('hadronic') decay channel of the gauge boson as described in the text. No b-tagging efficiencies are included here.

3.1.2 2HDM

As already alluded to earlier the parameter space of the general CP-conserving Type II 2HDM we are considering here is quite large as it depends on seven independent parameters. In order to get a feeling for the dependence of the signal cross-section of process (1) upon them, we present in Fig. 4 the results of our selected mass scenarios where we scan the allowed parameter space over 1000 randomly chosen points.

Comparing with the cross-sections obtained in the MSSM we notice that in the 2HDM, see Fig. 4, they can be up to two orders of magnitude larger. The main differences are due to the fact that:

- the trilinear Higgs couplings are not restricted in size by SUSY relations;
- the different parameters can vary independently of each other.

At the same time the kinematic factors will be the same for a given set of masses and widths of the different Higgs bosons. Therefore, in those cases many features of the signal, such as differential distributions, will be similar to the MSSM even though the normalisation can be completely different. We also see from Fig. 4 that there is quite a strong dependence on the masses of the Higgs bosons, with the maximal cross-section essentially decreasing by one order of magnitude as the heavy Higgs boson masses are increased from the scenario with lowest masses considered to the one with the highest masses.

As it is clear from Fig. 5, the largest inclusive cross-sections are obtained from the resonant channel $H \to hh$, whereas the contributions from the $A \to Zh$ and $H^\pm \to W^\pm h$ channels at the most reach about 10–20 fb. It is also clear from the figures that, even though there are slight differences in the parametric dependencies of the three different resonant contributions, the overall picture is very similar in all cases.

Finally, we have also verified, though not shown, that the most promising signals are the ones where the $W^\pm$ decays leptonically, which is sensitive to both the $H^\pm \to W^\pm h$ and $H \to hh$ resonant enhancements, and possibly also the leptonic decay of the Z, which is sensitive to possible $A \to Zh$ and $H \to hh$ resonances, whereas it is evident that the hadronic decay channels will not be relevant phenomenologically since they are only a factor $\sim$ 2–5 larger than the leptonic ones, yet burdened by overwhelming QCD backgrounds[11].

3.2 Signal-to-Background Differential Analysis

The backgrounds that we have considered are as follows. In the case of process (1) for $V = W^\pm$, they are:

1. $Wb\bar{b}b\bar{b}$, irreducible (i.e., it has exactly the same particle content as the signal);
2. $t\bar{t}$, with two mistags (i.e., when two light-quark jets are erroneously classified as b-jets);
3. $Wb\bar{b}jj$, with two mistags;
4. $Wjjjj$, with four mistags;
5. $Whb\bar{b} \to Wb\bar{b}b\bar{b}$, irreducible and co-resonant (i.e., it resonates at the h mass, albeit only once, unlike the signal, which does so twice);
6. $Whjj \to Wb\bar{b}jj$, co-resonant with two mistags.

In the case of process (1) for $V = Z$, they are:

1. $Zb\bar{b}b\bar{b}$, irreducible;
2. $Zb\bar{b}jj$, with two mistags;
3. $Zjjjj$, with four mistags;
4. $Zhb\bar{b} \to Zb\bar{b}b\bar{b}$, irreducible and co-resonant;
5. $Zhjj \to Zb\bar{b}jj$, co-resonant with two mistags.

[11] Hence, we will not consider hadronic signatures any further in this study.

In all cases both QCD and EW channels were considered, as appropriate. The former by exploiting ALPGEN and the latter the HELAS subroutines (including all 2HDM background channels to the signal but not the interferences). We have however verified that, already after the acceptance and preselection cuts, the last two channels (5. and 6. for $V = W^\pm$ plus 4. and 5. for $V = Z$) are negligible in both cases, so that we have ignored them in the reminder of the analysis. In fact, also the backgrounds 4. for $V = W^\pm$ and 3. for $V = Z$ are very small so that they could be neglected in first approximation. We have however included them in our simulation. The backgrounds 3. for $V = W^\pm$ and 2. for $V = Z$ are similar both in magnitude and shape to the corresponding irreducible ones (i.e., 1. for both $V = W^\pm$ and $V = Z$) after taking into account the appropriate weights, including the b-tagging/rejection factors discussed previously, although for clarity we do not plot them. Further, notice that background 2. for $V = W^\pm$ is significant before the final selection cuts, so that we have included it in our simulations.

We start by investigating the differential structure of process (1) in the attempt to extract the contributions that are most sensitive to the λ_{Hhh}, $\lambda_{W^\pm H^\mp h} = \cos(\beta - \alpha)$, and $\lambda_{ZAh} = \cos(\beta - \alpha)$ couplings, respectively. (Unfortunately, we can anticipate already that our studies revealed impossible to extract the $h \to hh$ component of process (1).) To this end, we isolate in (3) the corresponding "resonant" contributions, more specifically σ_{33} for λ_{Hhh} and σ_{22} for $\lambda_{W^\pm H^\mp h}$ and λ_{ZAh}[12]. Note that this corresponds to the approximation that the respective final states are WH or ZH and $H^\pm h$ or Ah, with the consequent decays $H \to hh$, $H^\pm \to W^\pm h$ and $A \to Zh$, for the two different processes at hand in (1). We have then identified, for the three different mass scenarios 1.–3. introduced in Sect. 2, those differential spectra that show significant differences from the yield of all the backgrounds above.

In Figs. 6–9 the resulting distributions[13] after the primary cuts in eqs. (5)–(8) for the leptonic $W^\pm$ and Z decays are given in the 2HDM with heavy Higgs masses in the range from ≈ 200 GeV to ≈ 400 GeV, limited to the contributions from the resonances, $H \to hh$ (with the H produced in association with a $W^\pm$) in Fig. 6, $H^\pm \to hW^\pm$ in Fig. 7, $A \to Zh$ in Fig. 8 plus $H \to hh$ (with the H produced in association with a Z) in Fig. 9. Note that in Fig. 7, as well as in the following Figs. 10 and 12 and Tab. 4, only the two mass scenarios with $M_{H^\pm} = 310$, 410 GeV are shown since the results for the $M_{H^\pm} = 300$ GeV scenario is very similar to the one for $M_{H^\pm} = 310$ GeV. The plotted observables are as follows: $M_{bb}^{\rm min}$ – the minimal mass of any pair of b-jets, $M_{bb}^{\rm nmin}$ – the next-to-minimal mass of any pair of b-jets, $p_T^{h_1}$ – the transverse momentum of the reconstructed h containing the b-jet

[12]We have verified, through BRS tests, that, although such contributions are not separately gauge invariant, gauge violating effects always occur at the permille level over the kinematic regions we are interested in (again, modulo the usual $\mathcal{O}(\Gamma/M)$ effects).

[13]Notice that the normalisation in these figures is to unit area.

with highest transverse momentum, $p_T^W\,(p_T^Z)$ – the transverse momentum of the reconstructed $W(Z)$ boson. In general terms, in all cases, the larger the Higgs masses involved in the decay the more effective the use of the described observables for the isolation of the signals.

The shape of the plotted distributions, after accounting for correlations amongst the kinematic variables, leads to the following choice of "optimised cuts" in order to enhance the signals of interest compared to the backgrounds trying to isolate the couplings λ_{Hhh}, $\lambda_{W^\pm H^\mp h}$ and λ_{ZAh}

- λ_{Hhh} from $q\bar{q}^{'} \to HW$ with $H \to hh$

$$M_{bb}^{\rm min} > 100 \text{ GeV}, \qquad M_{bb}^{\rm nmin} > 100 \text{ GeV}, \qquad p_T^{h_1} > 0 \text{ GeV}, \qquad p_T^W > 100 \text{ GeV} \quad (9)$$

- $\lambda_{W^\pm H^\mp h}$ from $q\bar{q}^{'} \to H^\pm h$ with $H^\pm \to hW^\pm$

$$M_{bb}^{\rm min} > 100 \text{ GeV}, \qquad M_{bb}^{\rm nmin} > 100 \text{ GeV}, \qquad p_T^{h_1} > 100 \text{ GeV}, \qquad p_T^W > 0 \text{ GeV} \quad (10)$$

- λ_{ZAh} from $q\bar{q} \to Ah$ with $A \to hZ$

$$M_{bb}^{\rm min} > 70 \text{ GeV}, \qquad M_{bb}^{\rm nmin} > 100 \text{ GeV}, \qquad p_T^{h_1} > 100 \text{ GeV}, \qquad p_T^Z > 0 \text{ GeV} \quad (11)$$

- λ_{Hhh} from $q\bar{q} \to HZ$ with $H \to hh$

$$M_{bb}^{\rm min} > 40 \text{ GeV}, \qquad M_{bb}^{\rm nmin} > 70 \text{ GeV}, \qquad p_T^{h_1} > 0 \text{ GeV}, \qquad p_T^Z > 100 \text{ GeV} \quad (12)$$

The resulting cross-sections for the relevant backgrounds after applying these optimised cuts are given in Tab. 2. After taking into account the b-tagging ($\epsilon_b = 0.5$) and mis-tagging ($R = 0.01$) factors, this means that only the $Vbbbb$ and $Vbbjj$ backgrounds are important, although in our numerical analysis we have kept all the discussed backgrounds.

In the next step of our analysis, we have scanned again the 2HDM parameter space in our three mass scenarios to search for points where, in presence of the above optimised cuts, one can establish a resonant signal at the 5σ level. Since the number of expected background events (B) is very small we have used Poisson statistics in way similar to the one suggested in [45] and calculated the number of signal events S that gives a probability for detecting $S + B$ or more events, given B expected ones, to be less than $2.8 \cdot 10^{-7}$ after $\int \mathcal{L} dt = 3000$ fb^{-1} of integrated luminosity, thus corresponding to a 5σ significance. The required signal cross-sections obtained in this way are given in Tab. 3.

The results of the scans are given in Figs. 10 and 11. From looking at the latter, there is obviously scope in finding a 5σ signal in almost all cases, for both the charged and neutral current version of process (1)[14], as shown in Figs. 10 and 11, respectively.

[14]The only notable exception is the $H^\pm \to hW^\pm$ resonance for $M_H = 250$ GeV, $M_h = 115$ GeV, $M_A = 220$ GeV and $M_{H^\pm} = 300$ GeV. This is due to the cut $M_{bb}^{\rm min} > 100$ GeV, which is necessary against the $t\bar{t}$ background but at the same time kills the signal in this case.

cut-comb	$\sigma(pp \to Wb\bar{b}b\bar{b})$ (fb)	$\sigma(pp \to Wb\bar{b}jj)$ (fb)	$\sigma(pp \to Wjjjj)$ (fb)	$\sigma(pp \to t\bar{t} \to Wb\bar{b}jj)$ (fb)
(9)	$9.2 \cdot 10^{-4}$	1.4	82	0.32
(10)	$1.8 \cdot 10^{-3}$	2.9	$1.6 \cdot 10^{2}$	0.59
cut-comb	$\sigma(pp \to Zb\bar{b}b\bar{b})$ (fb)	$\sigma(pp \to Zb\bar{b}jj)$ (fb)	$\sigma(pp \to Zjjjj)$ (fb)	
(11)	$3.9 \cdot 10^{-4}$	1.1	19	
(12)	$4.0 \cdot 10^{-4}$	1.2	20	

Table 2: Cross-sections for the most important background processes after the optimised cuts defined in (9)–(12), respectively, have been applied in addition to the acceptance and preselection cuts defined in (5)–(8). Note that b-tagging ($\epsilon_b = 0.5$) and mis-tagging ($R = 0.01$) factors have not been applied.

As it is clear from the plots the cross-sections with a $H^\pm \to W^\pm h$ or a $A \to Zh$ resonance are typically dominating the total cross-sections after the optimised cuts whereas the $H \to hh$ resonance is typically not dominant even after applying them. The reason for this is that the width of the A and $H^\pm$ are typically small in the 2HDM scenarios we are considering and thus these resonances always contribute significantly to the total cross-section. In contrast, the $H \to hh$ is typically wide and it cannot be small at the same time as the A or $H^\pm$ are wide.

Finally, Fig. 12 shows the phenomenal level of purity of the resonant signal samples that can be achieved, after the optimised cuts are implemented, for the "best case scenarios" in the 2HDM as given in Tab. 4. Note that here the signals have been calculated from the sum of all diagrams in (3) and thus all interferences are accounted for whereas the scenarios have been chosen to give the highest resonant cross-sections (the short-dashed lines in Figs. 10 and 11). The high purity is exemplified by the invariant masses that would enable the reconstruction of the decaying Higgs state, i.e., the four b-jet invariant mass (for the case of $H \to hh$) and the invariant mass of the Higgs h not containing the highest transverse momentum b-jet with the lepton-lepton (for the case $A \to hZ$) and lepton-neutrino (for the case $H^\pm \to hW^\pm$) pair. (Here, the $t\bar{t}$ background is not shown, as it has become totally negligible.) As a final note we have investigated how far the different "best case scenarios" in Table 4 are from the strong coupling limit. By applying the coupled renormalisation group evolution equations for the λ-couplings in Eq. (2) as well as the t, b, τ Yukawa couplings and the gauge couplings [46], we can determine how far a given point in parameter space can be

cut-comb	B	S	$\sigma(q\bar{q}^{'} \to Whh \to \ell\nu_\ell b\bar{b}b\bar{b})$ (fb)
(9)	0.30	6.1	0.033
(10)	0.59	7.3	0.041
cut-comb	B	S	$\sigma(q\bar{q} \to Zhh \to \ell\ell b\bar{b}b\bar{b})$ (fb)
(11)	0.16	5.1	0.027
(12)	0.16	5.1	0.027

Table 3: The number of background (B) events expected after $\int \mathcal{L}dt = 3000$ fb^{-1} of integrated luminosity when applying the optimised cuts defined in (9)–(12) (in addition to the acceptance and preselection cuts) and the number of signal (S) events that give a probability less than $2.8 \cdot 10^{-7}$ to observe $S + B$ events when expecting B events using Poisson statistics. In addition the corresponding signal cross-sections are given (without any b-tagging efficiency).

evolved in renormalisation scale before it reaches the tree-level unitarity limit [15]. This in turn gives an indication at what scale one can expect to see additional states and/or interactions (a.k.a. UV-completion). Applying this procedure we find that for most of the "best case scenarios", the tree-level unitarity limit is reached at a scale which is a factor 3-4 larger than the input scale. The only two exceptions are the two scenarios with $\sin(\beta - \alpha) = -0.01$ in Table 4 where this limit is reached only after evolving to a scale which is a factor $15 - 30$ times larger than the input scale.

4 Conclusions

In summary, we have shown the potential of a high luminosity LHC in extracting (resonant) decay signals of heavy Higgs states, both charged ($H^\pm$) and neutral (H and A), in a generic CP-conserving Type II 2HDM, using leptonic decays of a gauge boson and b-quarks ones of the lightest Higgs state of the model (h), the latter produced in the Higgs-strahlung process $q\bar{q}^{(')} \to Vhh$, with $V = W^\pm$ or Z and $q^{(')}$ referring to any possible (anti)quark flavour. The expanse of parameter space of the enlarged Higgs model that can be covered is sizable, not fine-tuned and yields detectable and extremely pure signals. This opens the prospect of accessing fundamental triple (Higgs and gauge) couplings of the model, notably λ_{Hhh} (but not λ_{hhh}) plus $\lambda_{W^\pm H^\mp h}$ and λ_{ZAh}, which would enable one to distinguish between this Higgs scenario and alternative ones (such as the MSSM) even in presence of degenerate mass and coupling spectra between the two. The possibility of extracting the latter and the precision

[15]We would like thank Oscar Stål for providing us with a code for solving the RGEs.

cut-comb (signal)	$\sin(\beta-\alpha)$	λ_5	$\tan\beta$	λ_{Hhh}	λ_{hhh}
$M_H = 250$ GeV, $M_A = 220$ GeV, $M_{H^\pm} = 300$ GeV					
(9) ($q\bar{q}' \to HW \to hhW$)	-0.82	-4.4	1.1	1259	1749
(10) ($q\bar{q}' \to H^\pm h \to hhW$)					
(11) ($q\bar{q} \to Ah \to hhZ$)	-0.72	-3.6	1.1	702	1805
(12) ($q\bar{q} \to HZ \to hhZ$)	0.73	-0.1	17.6	800	-1862
$M_H = 300$ GeV, $M_A = 305$ GeV, $M_{H^\pm} = 310$ GeV					
(9) ($q\bar{q}' \to HW \to hhW$)	-0.26	-2.9	0.9	-988	387
(10) ($q\bar{q}' \to H^\pm h \to hhW$)	-0.01	-1.3	7.5	-335	-873
(11) ($q\bar{q} \to Ah \to hhZ$)	-0.01	-1.4	2.9	-397	161
(12) ($q\bar{q} \to HZ \to hhZ$)	0.09	-1.3	24	-992	-293
$M_H = 400$ GeV, $M_A = 405$ GeV, $M_{H^\pm} = 410$ GeV					
(9) ($q\bar{q}' \to HW \to hhW$)	0.73	-0.7	5.2	867	-1328
(10) ($q\bar{q}' \to H^\pm h \to hhW$)	0.0034	-2.5	7.5	-671	68
(11) ($q\bar{q} \to Ah \to hhZ$)	-0.0012	-2.5	6.4	-651	58
(12) ($q\bar{q} \to HZ \to hhZ$)	0.73	-0.7	5.2	867	-1328

Table 4: The respective best case scenarios used for illustration in Fig. 12, after the implementation of the optimised cuts defined in (9)–(12). Note that there is no entry for the $H^\pm$ resonant scenario for $M_{H^\pm} = 300$ GeV since the results are very similar to the ones for $M_{H^\pm} = 310$ GeV.

at which this can be achieved, depending on the parameter space regions considered, ought to be assessed in a full detector environment, in presence of all necessary parton shower and hadronisation effects. However, the level of sophistication of our study and the encouraging results obtained hint at the feasibility of these analyses. To confirm this, we make available upon request all our codes.

Acknowledgments

SM thanks the Royal Society (London, UK) for partial financial support during one of his visits to Uppsala and so does JR for a visit to Southampton. RP acknowledges the financial support of MICINN under contract FPA2008-02984 and of the RTN European Programme MRTN-CT-2006-035505 (HEPTOOLS, Tools and Precision Calculations for Physics Discoveries at Colliders). SM acknowledges the latter too for partial funding. FP and MM thank the CERN Theory Unit for partial support. SM is financially supported in part by

the scheme 'Visiting Professor - Azione D - Atto Integrativo tra la Regione Piemonte e gli Atenei Piemontesi'. RP, FP and MM acknowledge the financial support of the bilateral INFN/MICINN program ACI2009-1045 (Aspects of Higgs physics at the LHC).

References

[1] J.F. Gunion, H.E. Haber, G.L. Kane and S. Dawson, "The Higgs Hunter Guide" (Addison-Wesley, Reading MA, 1990), Erratum, `hep-ph/9302272`.

[2] A. Djouadi, hep-ph/0503172; hep-ph/0503173. A. Djouadi, Phys. Rept. **457** (2008) 1 [arXiv:hep-ph/0503172]; Phys. Rept. **459** (2008) 1 [arXiv:hep-ph/0503173].

[3] ATLAS collaboration, 'ATLAS Technical proposal', CERN/LHCC/94-43, LHCC/P2, 1994; ATLAS Detector and Physics Performance Technical Design Report, ATLAS TDR 14, CERN/LHCC 99-14, 1999, "Expected Performance of the ATLAS Experiment - Detector, Trigger and Physics," arXiv:0901.0512 [hep-ex].

[4] CMS collaboration, 'CMS Technical proposal', CERN/LHCC/94-38, LHCC/P1, 1994; 'CMS Physics Technical Design Report, Volume I: Detector Performance and Software' CMS TDR 8.1, CERN/LHCC 2006-001, 2006.

[5] T. Aaltonen *et al.* [CDF and D0 Collaborations], Phys. Rev. Lett. **104** (2010) 061802, arXiv:1001.4162 [hep-ex].

[6] J.F. Gunion and H.E. Haber, Phys. Rev. **D67** (2003) 075019.

[7] F. Boudjema and A.V. Semenov, Phys. Rev. **D66** (2002) 095007.

[8] M. Moretti, S. Moretti, F. Piccinini, R. Pittau and A.D. Polosa, JHEP **02** (2005) 04; `hep-ph/0411039`.

[9] M. Moretti, S. Moretti, F. Piccinini, R. Pittau and J. Rathsman, JHEP **0712** (2007) 075, arXiv:0706.4117 [hep-ph].

[10] G. Ferrera, J. Guasch, D. Lopez-Val and J. Sola, Phys. Lett. B **659** (2008) 297 [arXiv:0707.3162 [hep-ph]].

[11] F. Gianotti, M.L. Mangano and T. Virdee (conveners), `hep-ph/0204087`.

[12] V. Barger, T. Han and R.J.N. Phillips, Phys. Rev. **D38** (1988) 2766.

[13] A. Djouadi, W. Kilian, M. Muhlleitner and P.M. Zerwas, Eur. Phys. J. **C10** (1999) 45.

[14] http://durpdg.dur.ac.uk/hepdata/pdf.html.

[15] M.L. Mangano, M. Moretti, F. Piccinini, R. Pittau and A.D. Polosa, JHEP **07** (2003) 001.

[16] H. Murayama, I. Watanabe and K. Hagiwara, KEK Report 91–11, January 1992.

[17] G.P. Lepage, J. Comp. Phys. **27** (1978) 192, preprint CLNS-80/447, March 1980.

[18] H. Kharraziha and S. Moretti, Comp. Phys. Comm. **127** (2000) 242; Erratum, ibidem **134** (2001) 136.

[19] M. Carena, P.H. Chankowski, S. Pokorski and C.E.M. Wagner, Phys. Lett. **B441** (1998) 205.

[20] A. Djouadi, J. Kalinowski and M. Spira, Comp. Phys. Comm. **108** (1998) 56.

[21] F. Mahmoudi and O. Stal, Phys. Rev. D **81** (2010) 035016 [arXiv:0907.1791 [hep-ph]].

[22] O. Deschamps, S. Descotes-Genon, S. Monteil, V. Niess, S. T'Jampens and V. Tisserand, arXiv:0907.5135 [hep-ph].

[23] A.G. Akeroyd, A. Arhrib and E.M. Naimi, Phys. Lett. **B490** (2000) 119.

[24] I. F. Ginzburg and I. P. Ivanov, Phys. Rev. D **72** (2005) 115010.

[25] E. W. N. Glover and J. J. van der Bij, Nucl. Phys. B **309** (1988) 282.

[26] D. A. Dicus, C. Kao and S. S. D. Willenbrock, Phys. Lett. B **203** (1988) 457.

[27] J. Dai, J. F. Gunion and R. Vega, its Phys. Lett. B **371** (1996) 71.

[28] J. Dai, J. F. Gunion and R. Vega, Phys. Lett. B **387** (1996) 801.

[29] T. Plehn, M. Spira and P. M. Zerwas, Collisions," Nucl. Phys. B **479** (1996) 46 [Erratum-ibid. B **531** (1998) 655].

[30] S. Moretti, J. Phys. G **28** (2002) 2567.

[31] U. Baur, T. Plehn and D. L. Rainwater, Phys. Rev. D **67** (2003) 033003

[32] U. Baur, T. Plehn and D. L. Rainwater, Phys. Rev. D **69** (2004) 053004

[33] U. Baur, T. Plehn and D. L. Rainwater, Phys. Rev. D **68**, 033001 (2003) [arXiv:hep-ph/0304015].

[34] S. Moretti and J. Rathsman, Eur. Phys. J. **C33** (2004) 41.

[35] G. D. Kribs, T. Plehn, M. Spannowsky and T. M. P. Tait, Phys. Rev. D **76** (2007) 075016 [arXiv:0706.3718 [hep-ph]].

[36] A. Arhrib, R. Benbrik, R.B. Guedes and R. Santos, Phys. Rev. **D78** (2008) 075002.

[37] A. Arhrib, R. Benbrik, C. H. Chen, R. Guedes and R. Santos, JHEP **0908** (2009) 035 [arXiv:0906.0387 [hep-ph]].

[38] D. Lopez-Val and J. Sola, Phys. Rev. D **81**, 033003 (2010) [arXiv:0908.2898 [hep-ph]].

[39] R. N. Hodgkinson, D. Lopez-Val and J. Sola, Phys. Lett. B **673**, 47 (2009) [arXiv:0901.2257 [hep-ph]].

[40] N. Bernal, D. Lopez-Val and J. Sola, Phys. Lett. B **677** (2009) 39 [arXiv:0903.4978 [hep-ph]].

[41] S. Moretti and W.J. Stirling, Phys. Lett. **B347** (1995) 291, Erratum, ibidem **B366** (1996) 451; S. Kanemura, S. Moretti, Y. Mukai, R. Santos and K. Yagyu, arXiv:0901.0204 [hep-ph].

[42] D. Eriksson, J. Rathsman and O. Stål, Comput. Phys. Commun. **181** (2010) 189, arXiv:0902.0851 [hep-ph], `http://www.isv.uu.se/thep/MC/2HDMC/`

[43] D. Lopez-Val, J. Sola and N. Bernal, Phys. Rev. D **81** (2010) 113005 [arXiv:1003.4312 [hep-ph]].

[44] See: `http://lephiggs.web.cern.ch/LEPHIGGS/papers/`.

[45] S.I. Bityukov and N.V. Krasnikov, Nucl. Instr. and Meth. **A452** (2000) 518.

[46] P. M. Ferreira, D. R. T. Jones, JHEP **0908** (2009) 069. [arXiv:0903.2856 [hep-ph]].

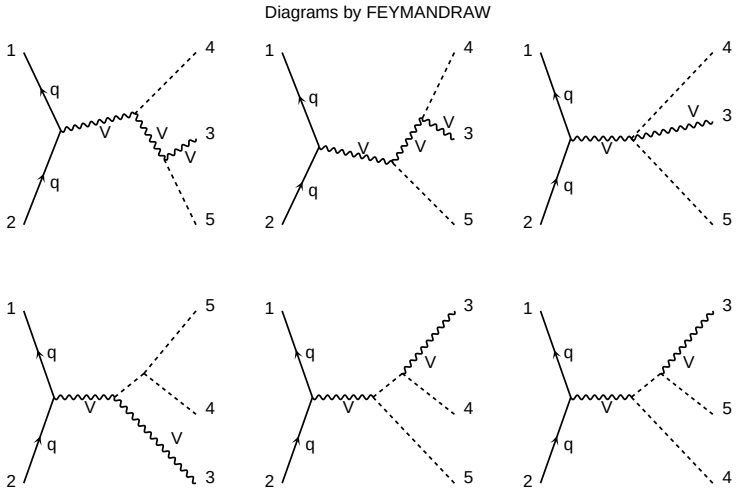

Figure 1: Feynman diagrams for $q_1\bar{q}_2^{(\prime)} \to V_3 h_4 h_5$.

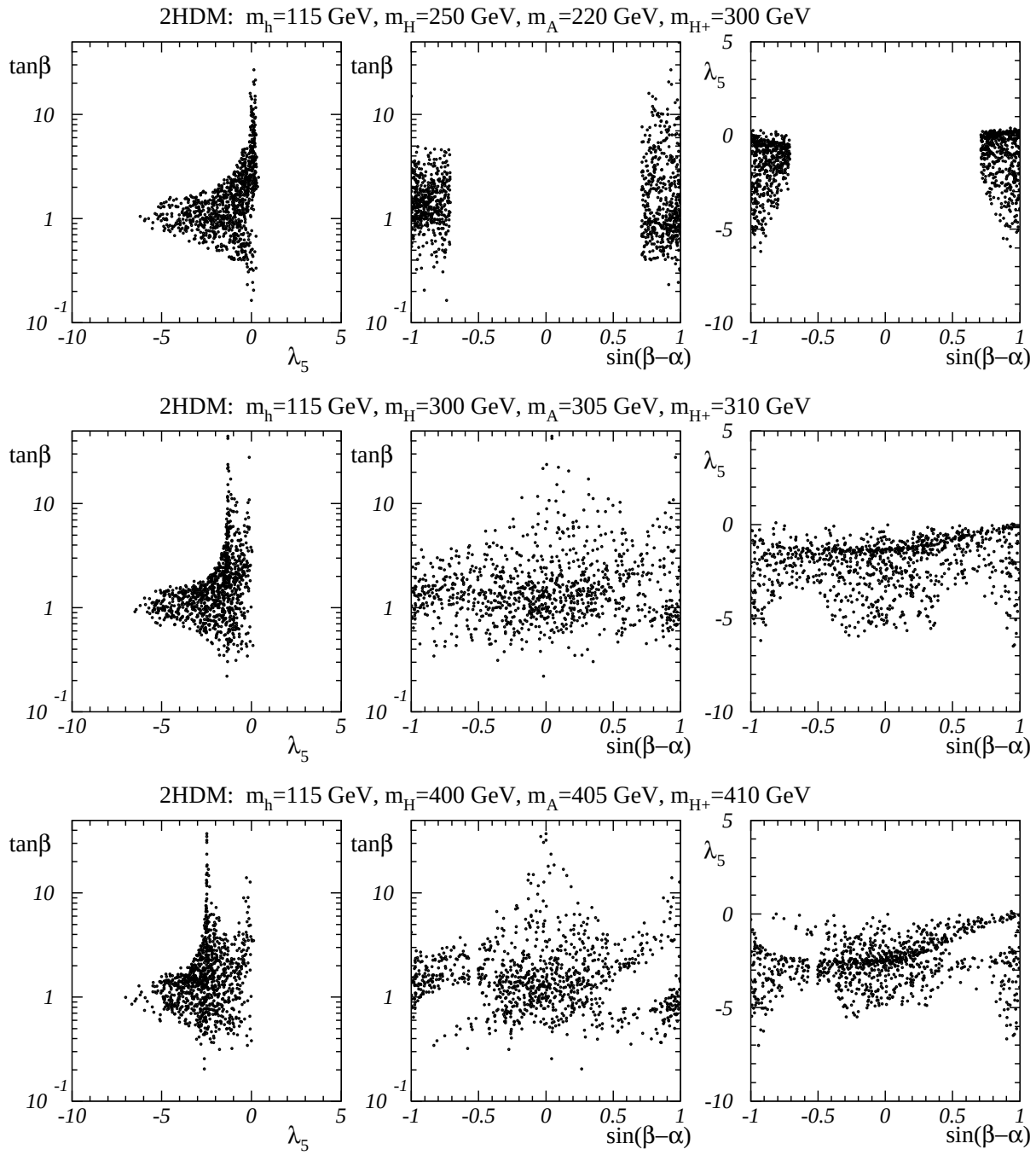

Figure 2: The projection of the allowed points in the 2HDM parameter space on three different planes, λ_5–$\tan\beta$, $\sin(\beta-\alpha)$–$\tan\beta$ and $\sin(\beta-\alpha)$–λ_5, in the three different mass scenarios: (top) $M_H = 250$ GeV, $M_h = 115$ GeV, $M_A = 220$ GeV and $M_{H^\pm} = 300$ GeV, (middle) $M_H = 300$ GeV, $M_h = 115$ GeV, $M_A = 305$ GeV and $M_{H^\pm} = 310$ GeV, (bottom) $M_H = 400$ GeV, $M_h = 115$ GeV, $M_A = 405$ GeV and $M_{H^\pm} = 410$ GeV. The projections have been obtained with a sample of 1000 random points in the allowed 2HDM parameter space.

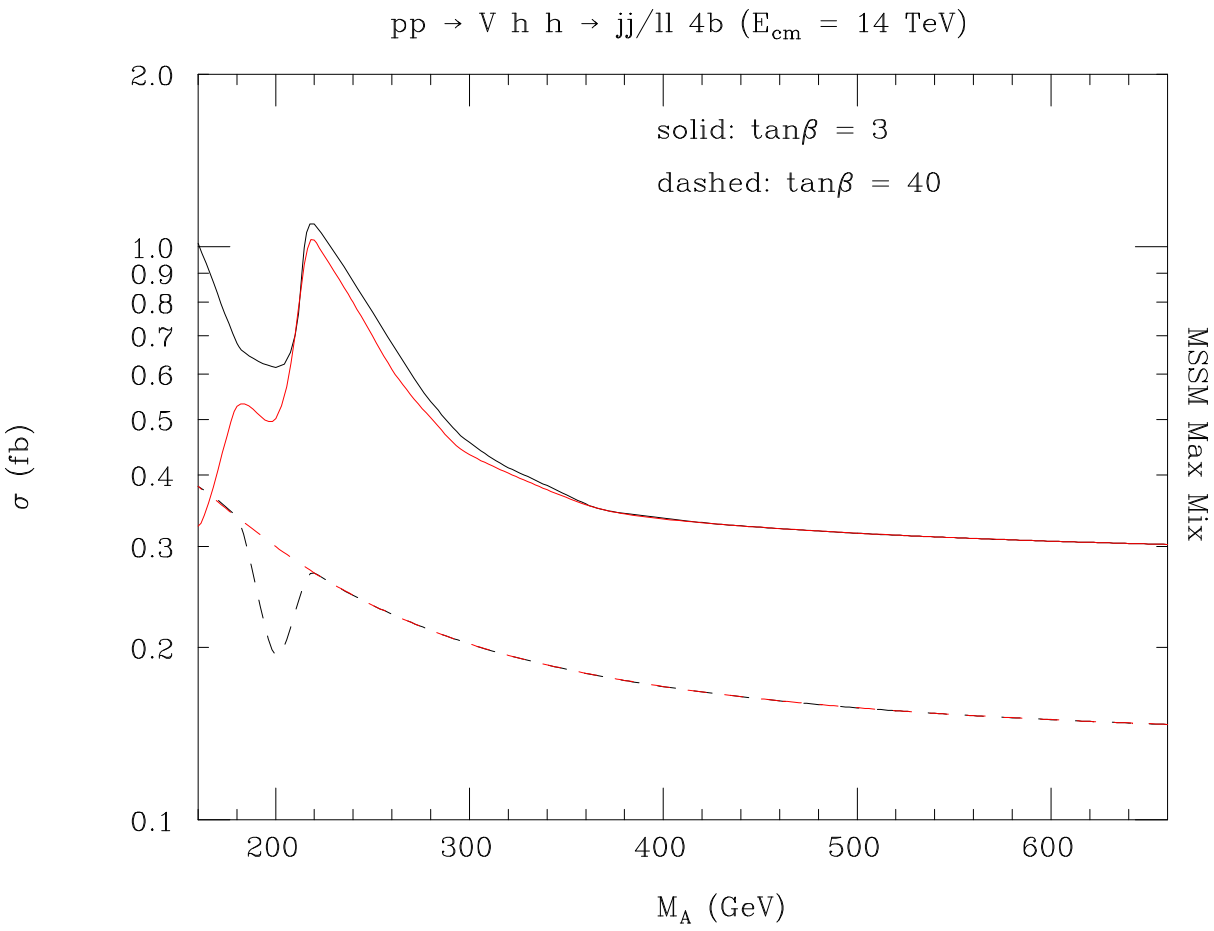

Figure 3: The inclusive cross-sections (as defined in the text) for Higgs-strahlung in (1), followed by $hh \to b\bar{b}b\bar{b}$ and $V \to$ 'anything' decays, as a function of the CP-odd Higgs boson mass, M_A, for two choices of $\tan\beta$, assuming the MSSM in Maximal Mixing configuration. The red lines correspond to the case in which we have removed from the computation the last two Feynman diagrams in the previous figure.

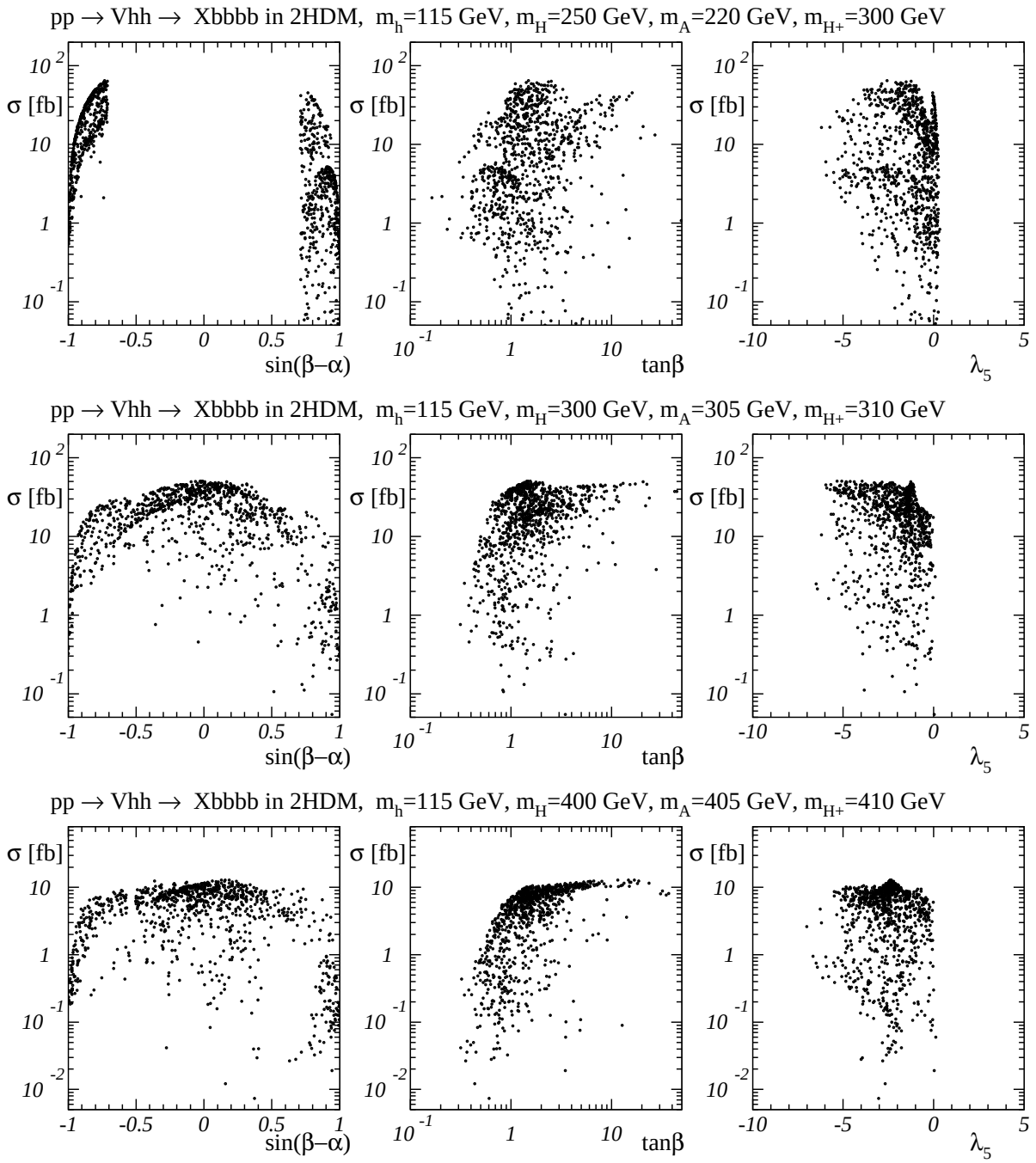

Figure 4: The inclusive cross-section in the 2HDM (as defined in the text) for Higgs-strahlung in (1), followed by $hh \to b\bar{b}b\bar{b}$ and $V \to$ 'anything' decays in the three different mass scenarios: (top) $M_H = 250$ GeV, $M_h = 115$ GeV, $M_A = 220$ GeV and $M_{H^\pm} = 300$ GeV, (middle) $M_H = 300$ GeV, $M_h = 115$ GeV, $M_A = 305$ GeV and $M_{H^\pm} = 310$ GeV, (bottom) $M_H = 400$ GeV, $M_h = 115$ GeV, $M_A = 405$ GeV and $M_{H^\pm} = 410$ GeV, as a function of the remaining three parameters, for 1000 random points in the allowed 2HDM parameter space.

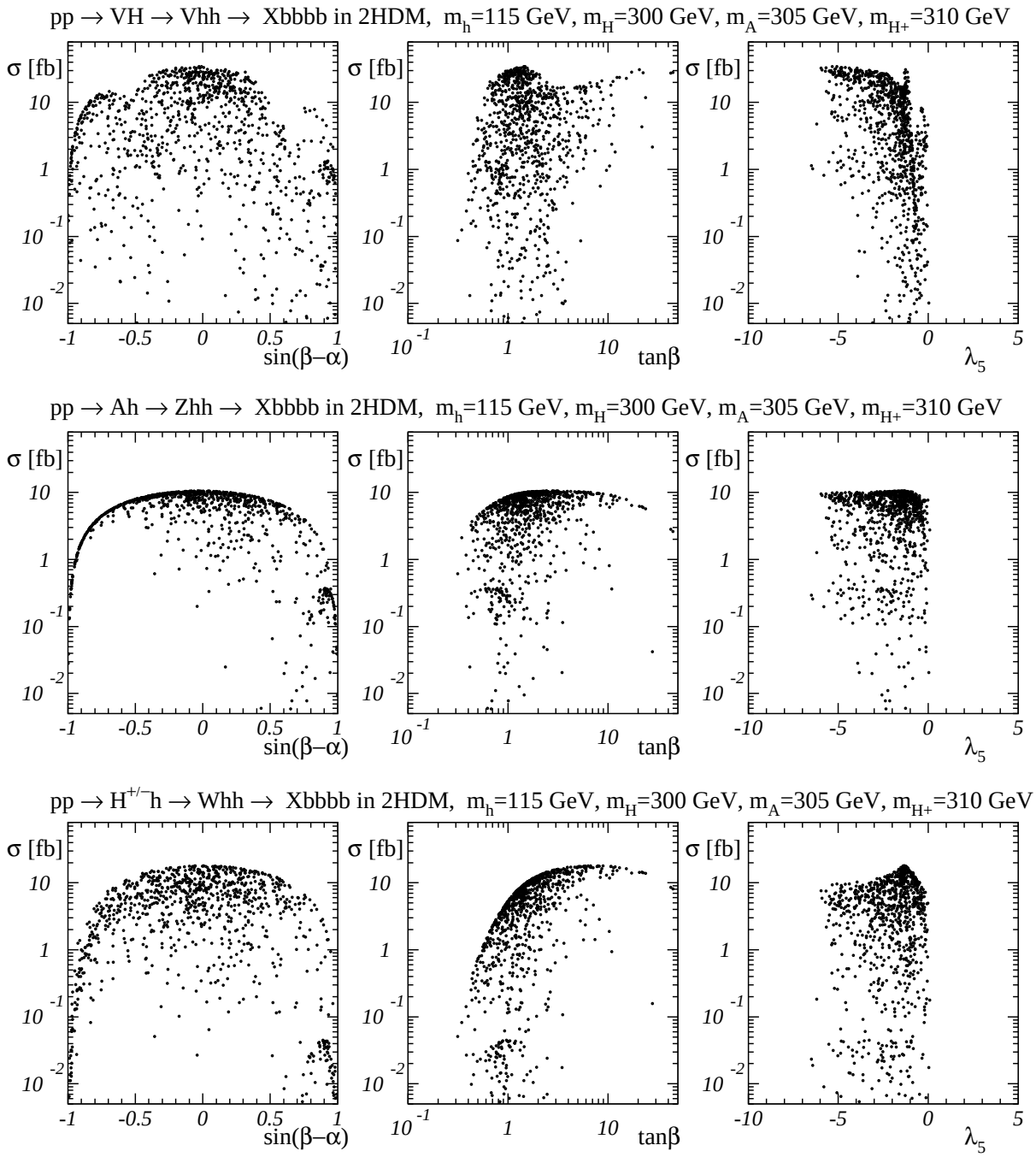

Figure 5: The contributions to the inclusive cross-section in the 2HDM (as defined in the text) for Higgs-strahlung in (1), followed by $hh \to b\bar{b}b\bar{b}$ and $V \to$ 'anything' decays from the: (top) $H \to hh$, (middle) $A \to Zh$, and (bottom) $H^{\pm} \to W^{\pm}h$, channels respectively in the mass scenario: $M_H = 300$ GeV, $M_h = 115$ GeV, $M_A = 305$ GeV and $M_{H^{\pm}} = 310$ GeV, as a function of the remaining three parameters, for 1000 random points in the allowed 2HDM parameter space.

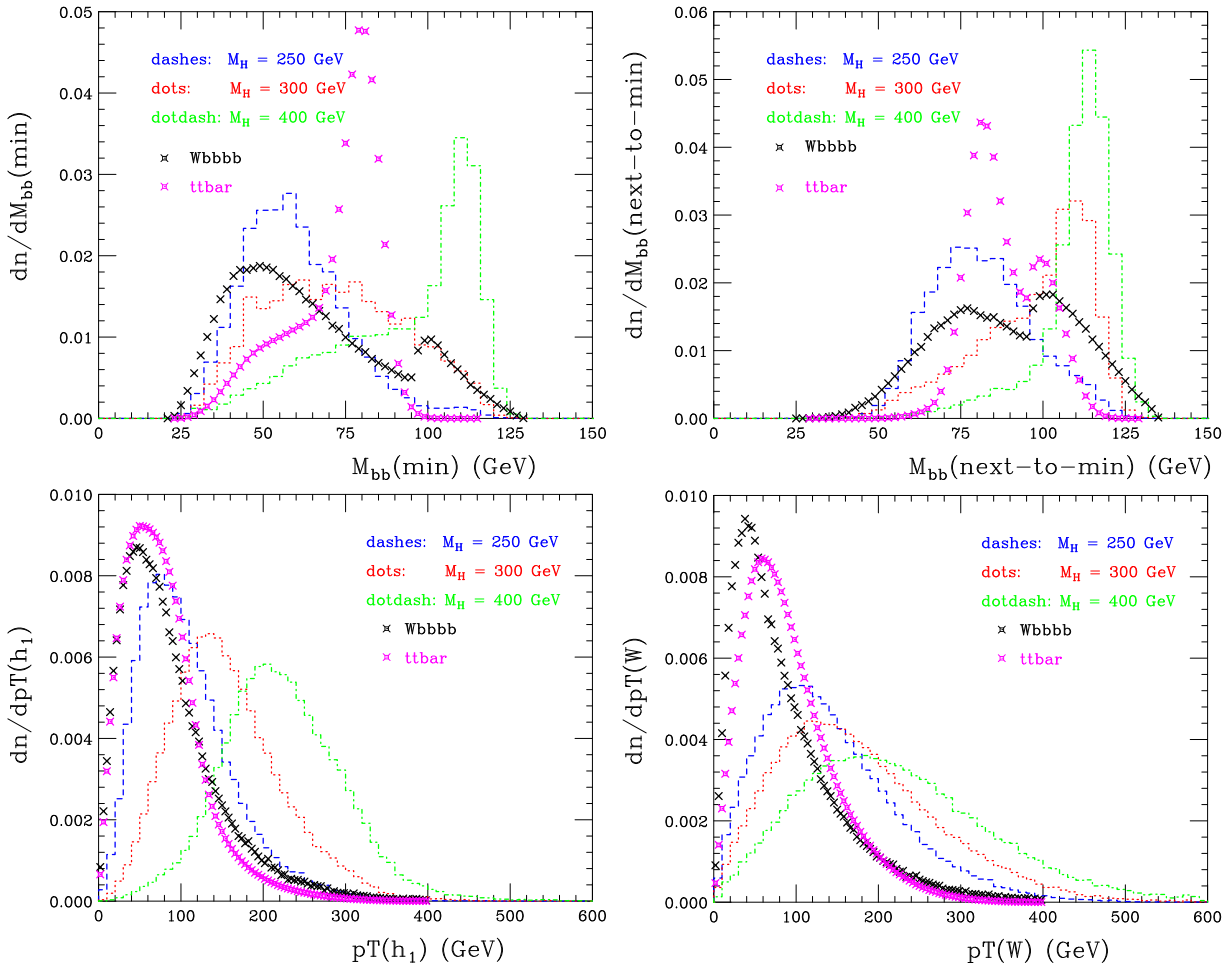

Figure 6: Differential distributions (normalised to unit area) of the $H \to hh$ contribution to Higgs-strahlung (solid lines) after the primary cuts of eqs. (5)–(8) in the 2HDM (as defined in the text) followed by $hh \to b\bar{b}b\bar{b}$ and $W^{\pm} \to \ell\nu_{\ell}$ decays in the different mass scenarios indicated. Background spectra from the $Wbbbb$ and $t\bar{t}$ processes are also given (crosses). The distributions are as follows: the minimum bb invariant mass (top left); the next-to-minimum bb invariant mass (top right); the transverse momentum of the reconstructed Higgs boson containing the b-jet with largest transverse momentum (bottom left); the transverse momentum of the reconstructed $W^{\pm}$ (bottom right).

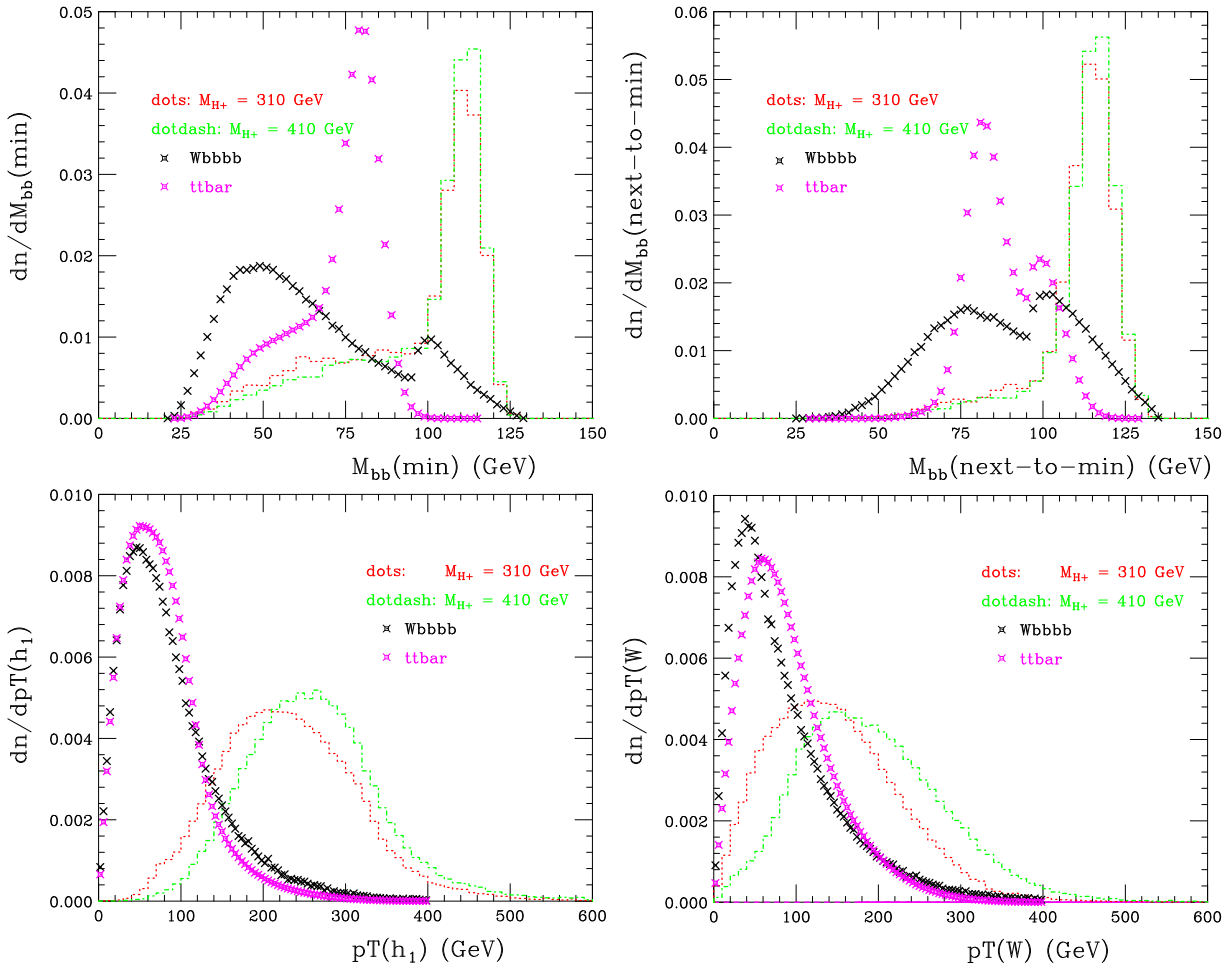

Figure 7: Differential distributions (normalised to unit area) of the $H^\pm \to hW^\pm$ contribution to Higgs-strahlung (solid lines) after the primary cuts of eqs. (5)–(8) in the 2HDM (as defined in the text) followed by $hh \to b\bar{b}b\bar{b}$ and $W^\pm \to \ell\nu_\ell$ decays in the different mass scenarios indicated. Background spectra from the $Wbbbb$ and $t\bar{t}$ processes are also given (crosses). The distributions are as follows: the minimum bb invariant mass (top left); the next-to-minimum bb invariant mass (top right); the transverse momentum of the reconstructed Higgs boson containing the b-jet with largest transverse momentum (bottom left); the transverse momentum of the reconstructed $W^\pm$ (bottom right).

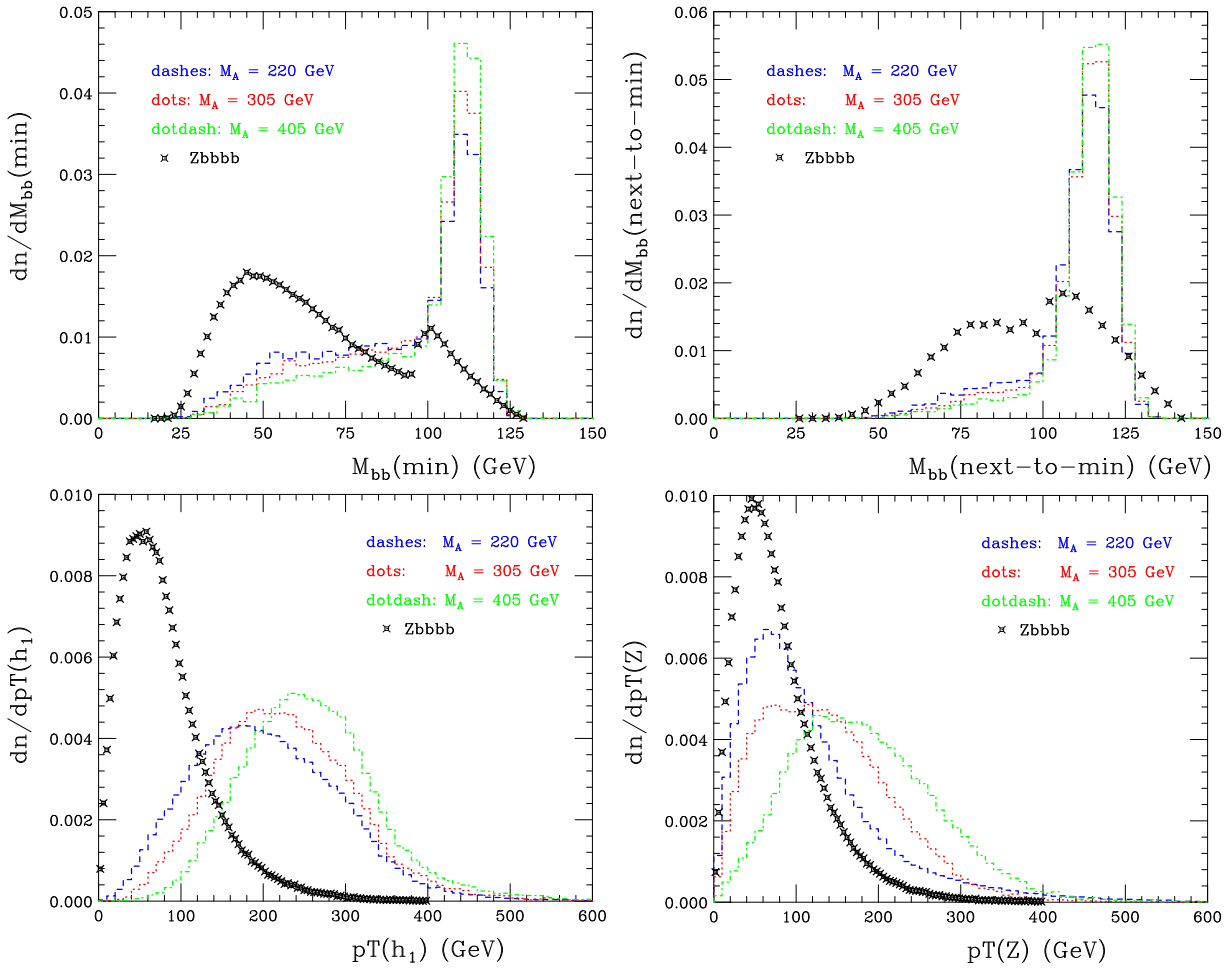

Figure 8: Differential distributions (normalised to unit area) of the $A \to hZ$ contribution to Higgs-strahlung (solid lines) after the primary cuts of eqs. (5)–(8) in the 2HDM (as defined in the text) followed by $hh \to b\bar{b}b\bar{b}$ and $Z \to \ell\ell$ decays in the different mass scenarios indicated. Background spectra from the dominant irreducible background $Zbbbb$ are also given (crosses). The distributions are as follows: the minimum bb invariant mass (top left); the next-to-minimum bb invariant mass (top right); the transverse momentum of the reconstructed Higgs boson containing the b-jet with largest transverse momentum (bottom left); the transverse momentum of the reconstructed Z (bottom right).

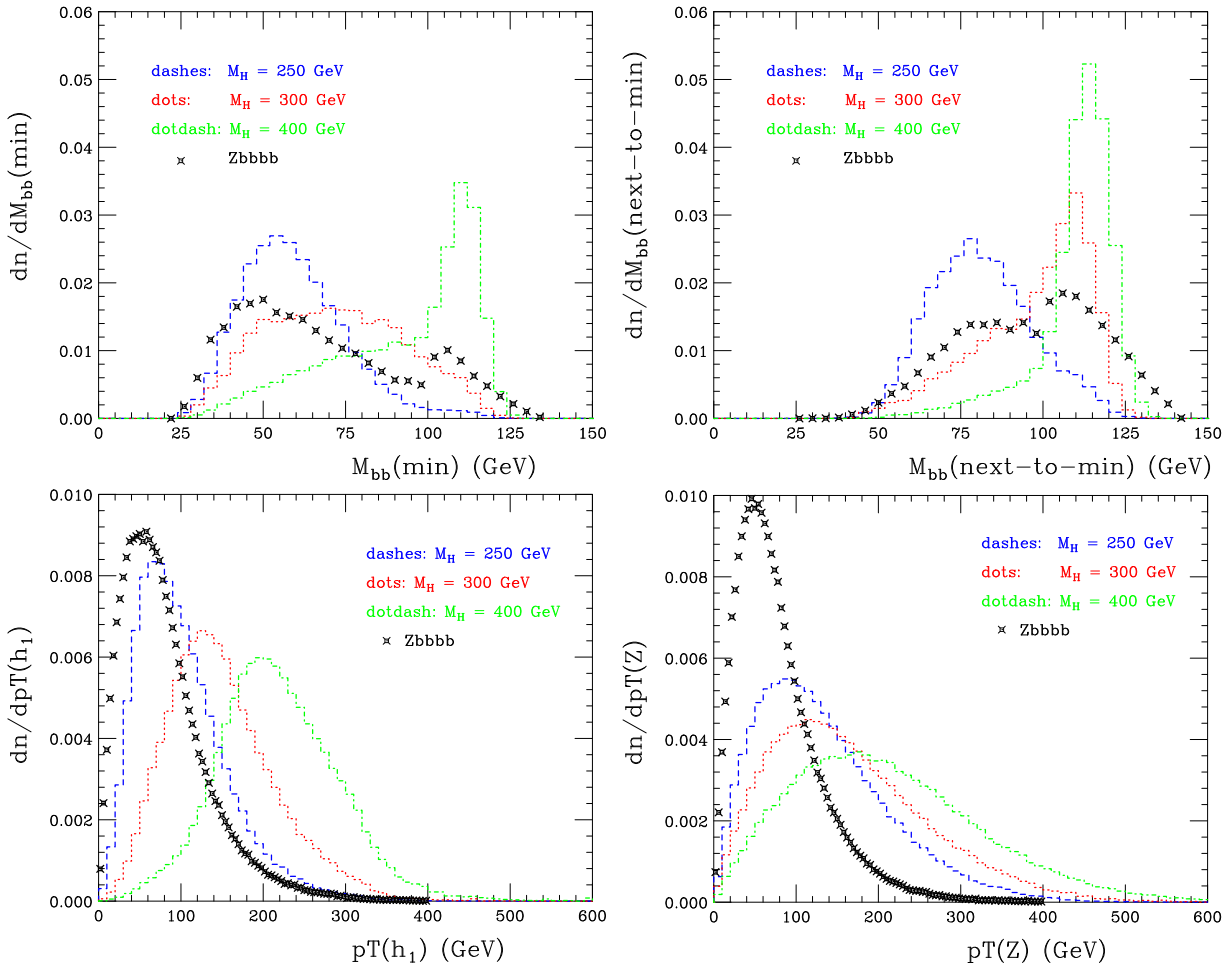

Figure 9: Differential distributions (normalised to unit area) of the $H \to hh$ contribution to Higgs-strahlung (solid lines) after the primary cuts of eqs. (5)–(8) in the 2HDM (as defined in the text) followed by $hh \to b\bar{b}b\bar{b}$ and $Z \to \ell\ell$ decays in the different mass scenarios indicated. Background spectra from the dominant irreducible background $Zbbbb$ are also given (crosses). The distributions are as follows: the minimum bb invariant mass (top left); the next-to-minimum bb invariant mass (top right); the transverse momentum of the reconstructed Higgs boson containing the b-jet with largest transverse momentum (bottom left); the transverse momentum of the reconstructed Z (bottom right).

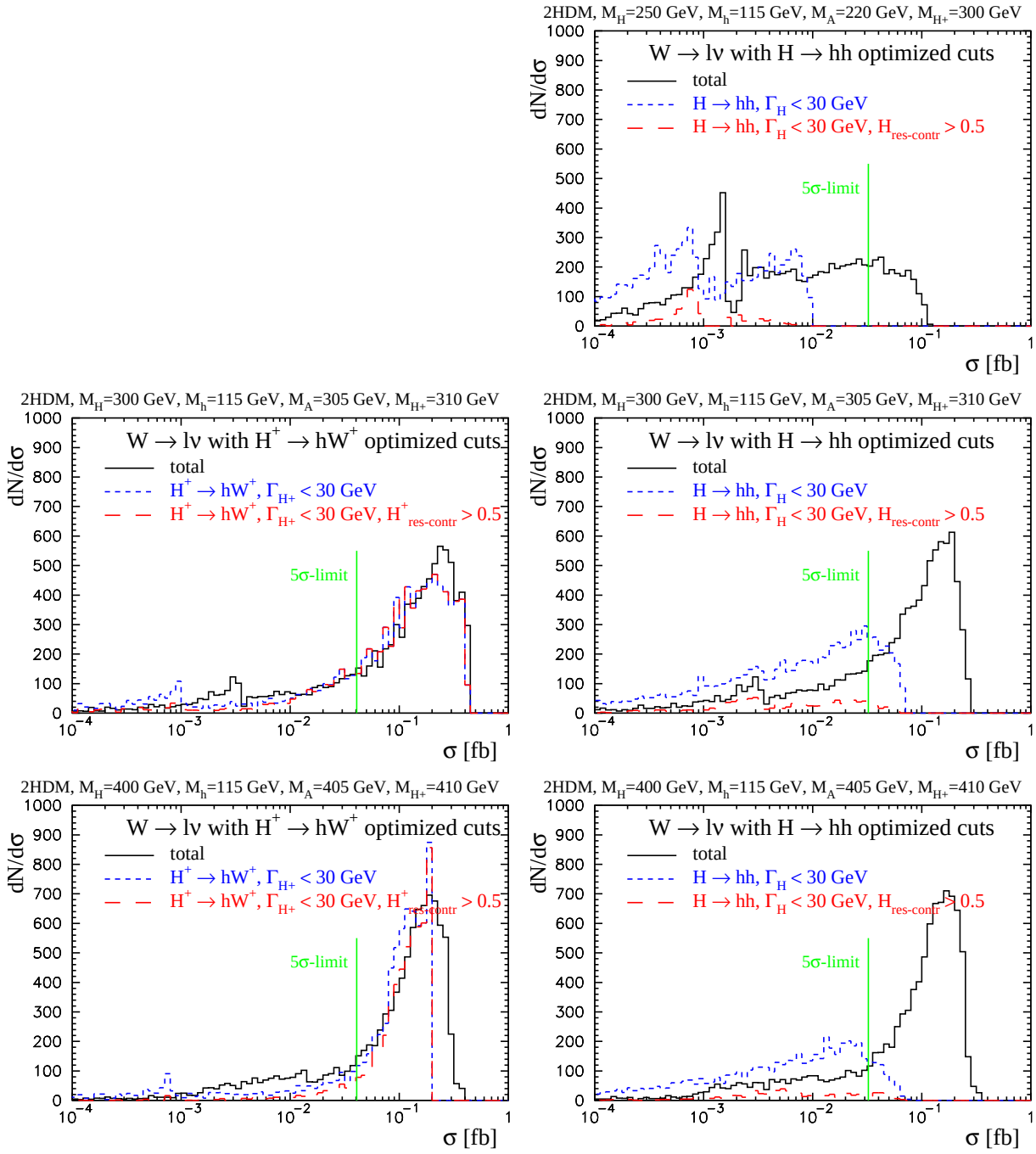

Figure 10: Distribution of resulting cross-sections in the 2HDM with leptonic $W^{\pm}$ decays when scanning over 10000 parameter space points for the different mass scenarios indicated. The two columns show the resulting cross-sections after applying optimal cuts (as defined in the text) to select the $H^{\pm} \to hW^{\pm}$ (left) or $H \to hh$ (right) channels respectively. The different lines show: the inclusive cross-section (solid), the cross-section corresponding to the $H^{\pm} \to hW^{\pm}$ (left) or $H \to hh$ (right) resonances (dashed blue), and the same cross-section when requiring that the contributions from the resonance is at least 50% (red long dash).

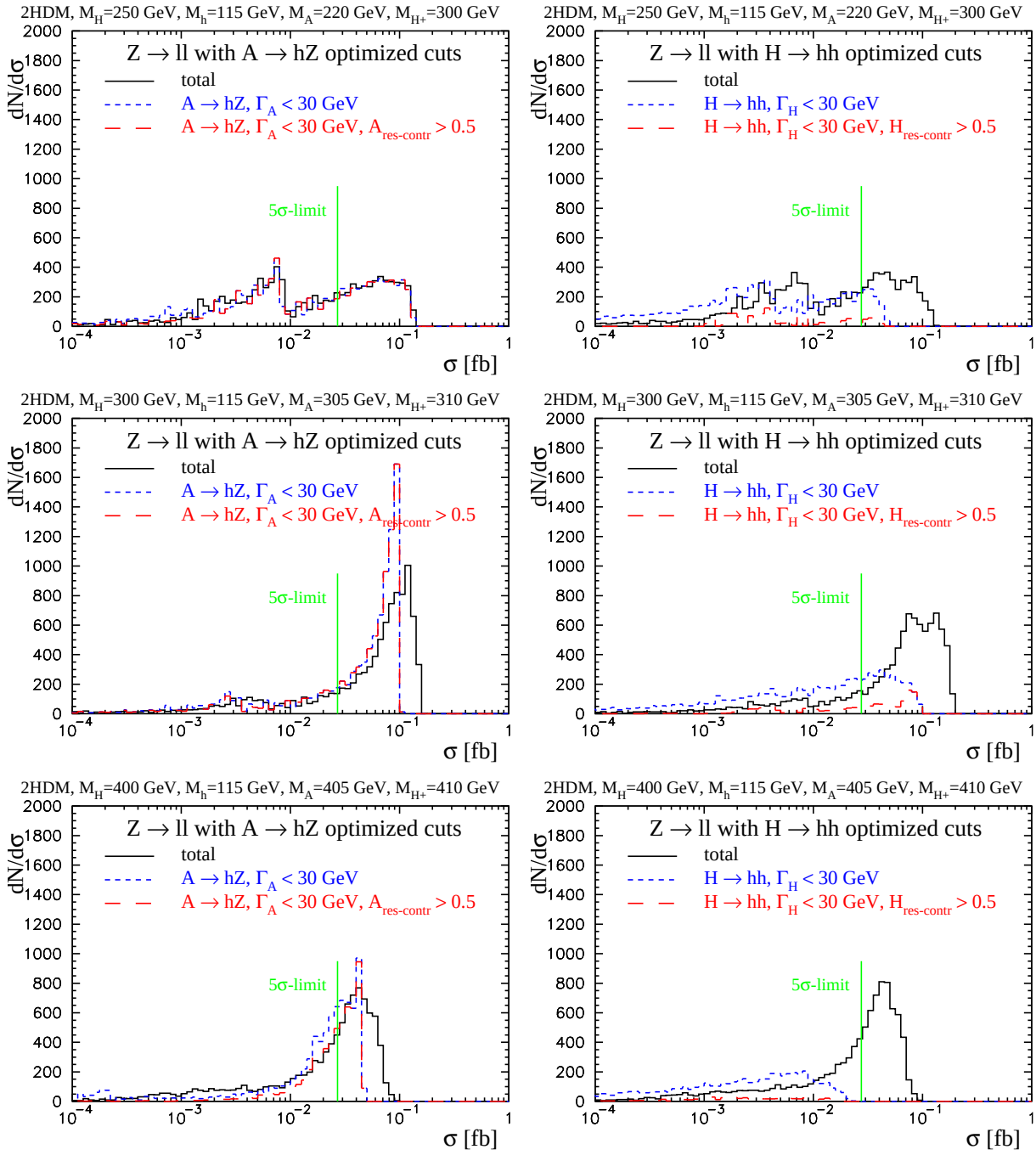

Figure 11: Distribution of resulting cross-sections in the 2HDM with leptonic Z decays when scanning over 10000 parameter space points for the different mass scenarios indicated. The two columns show the resulting cross-sections after applying optimal cuts (as defined in the text) to select the $A \to hZ$ (left) or $H \to hh$ (right) channels respectively. The different lines show: the inclusive cross-section (solid), the cross-section corresponding to the $A \to hZ$ (left) or $H \to hh$ (right) resonances (dashed blue), and the same cross-section when requiring that the contributions from the resonance is at least 50% (red long dash).

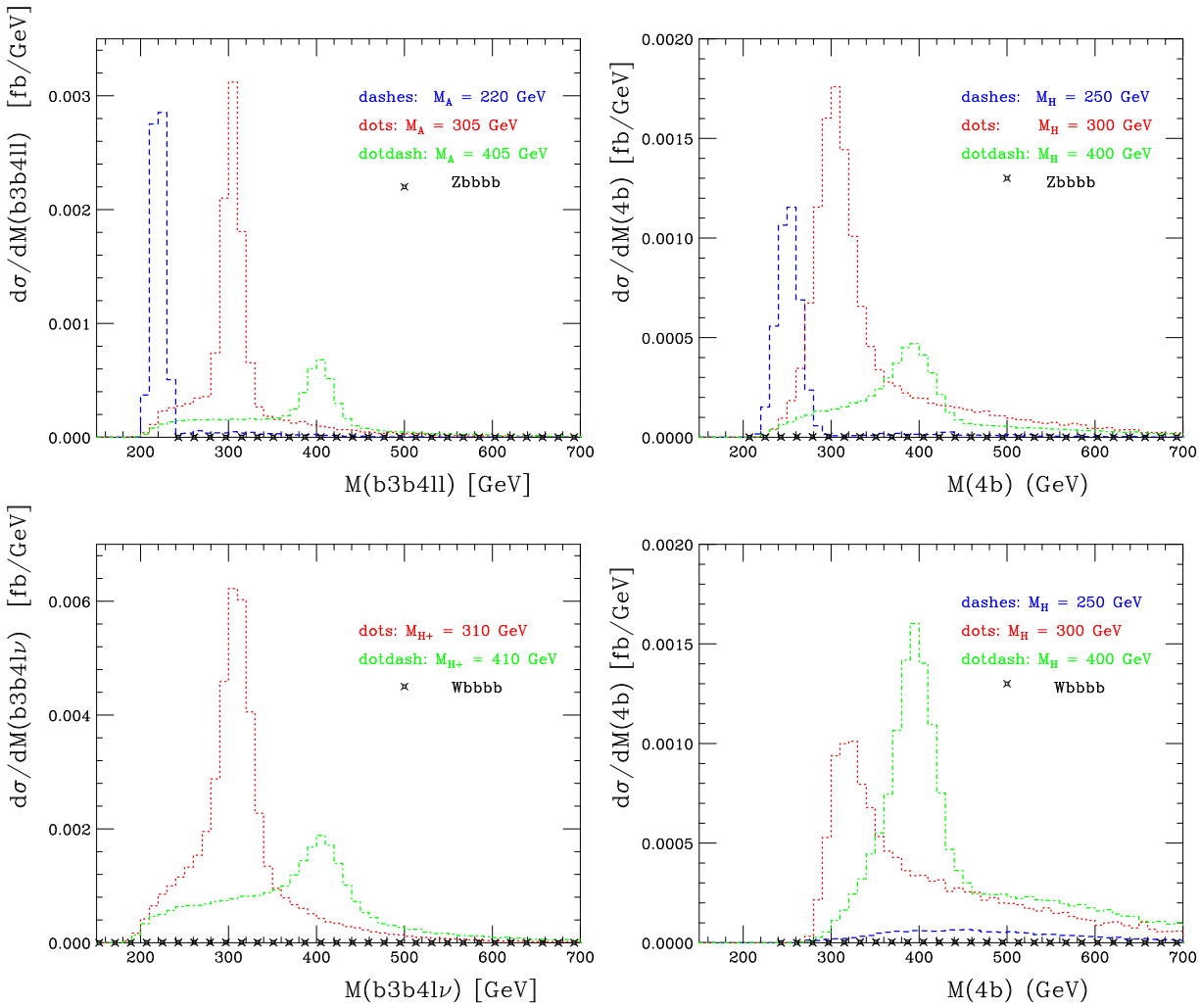

Figure 12: Differential distributions (normalised to the cross-sections in the respective "best case scenarios") after the optimised cuts for the four different signals: $pp \to Ah$ with $A \to hZ$ (top left); $pp \to ZH$ with $H \to hh$ (top right); $pp \to H^{\pm}h$ with $H^{\pm} \to hW^{\pm}$ (bottom left); $pp \to WH$ with $H \to hh$ (bottom right). The distributions are as follows: the invariant mass of the reconstructed A boson using the second reconstructed h (top left); the invariant mass of the reconstructed H boson (top right); the invariant mass of the reconstructed $H^{\pm}$ boson using the second reconstructed h (bottom left); the invariant mass of the reconstructed H boson (bottom right).